Soft laser-plasma X-ray source for differential absorption imaging of tracing elements in thin samples

L. A. GIZZI,[1] C.A. CECCHETTI,[1] M. GALIMBERTI,[1] D. GIULIETTI,[1,2] A. GIULIETTI,[1]
P. KOESTER,[1] L. LABATE,[1,3] S. LAVILLE,[1] AND P. TOMASSINI[1]

[1]Intense Laser Irradiation Laboratory, IPCF, Area della Ricerca CNR, Pisa, Italy
[2]Also at Dipartimento di Fisica, Università di Pisa and INFN, Pisa, Italy
[3]Also at Dipartimento di Fisica, Università di Bologna, Bologna, Italy

Abstract

The differential imaging technique is particularly suitable for the detection of small concentrations of contrasts agents for biological and medical applications in samples using X-ray radiography. In this paper, we present an application of this technique using a laser-plasma soft X-ray source combined with a bent crystal. Using a Fresnel plate as a test object, we were able to obtain spatial resolutions of the order of a few tens of microns. The use of our configuration to perform differential imaging of a test-sample at the L_2 edge of Br at 1,596 eV is finally demonstrated.

Keywords: Differential imaging; Laser-plasma; X-ray absorption

1. INTRODUCTION

The detection of specific elements or compounds in a sample is a task of a great interest in a wide range of fundamental and applied research fields. In some circumstances, information on the total concentration as well as on the spatial distribution of a given compound in a sample can be obtained by exploiting the self-emission properties of a specific radioactive tracing element included in the compound (Barbarics *et al.*, 1994). Alternatively, highly X-ray absorbing contrast agents are used in combination with radiographic imaging techniques that provide a two-dimensional (2D) mapping of the X-ray absorption in the sample (Suortti & Thomlinson, 2003). Techniques based upon these principles are currently used in a number of laboratory as clinical diagnostic techniques.

The differential absorption imaging technique is an alternative powerful tool for accomplishing this task that relies solely on the spectral properties of absorption of X-ray radiation by an atomic element. In particular, the technique takes advantage of the sharp change of the photon attenuation length across a chosen absorption edge of a given element.

The method has already been proposed for the detection of small concentrations of contrast agents for biological and medical applications. For instance, it is currently under study for clinical application in coronary angiography (Dill *et al.*, 1998). Up to now, such studies have been carried out using monochromatic radiation emitted from synchrotron sources (Suortti & Thomlinson, 2003). More recently, laser-plasma K_α sources have also been suggested as possible compact sources for this application (Tillman *et al.*, 1996; Andersson *et al.*, 2001).

In this paper, we present investigations aimed at scaling the application of this technique from the hard X-rays typically used for coronary angiography to the soft X-ray range. This allows to perform a quantitative elemental analysis of thin samples. In particular, we investigate the possibility of using a table-top laser-plasma soft X-ray source combined with the diffractive crystal properties for the development of a standard arrangement for a dedicated small-scale equipment.

A short basic introduction to the technique of differential absorption is first given, followed by the description of a preliminary experiment carried out using the PLX laser-plasma soft X-ray source developed (Marzi *et al.*, 2000) at the Intense Laser Irradiation Laboratory. We then show the results obtained by applying the differential imaging to a thin sample containing a solution of bromine.

Address correspondence and reprint requests to: L.A. Gizzi, IPCF, Intense Laser Irradiation Laboratory, CNR, Via Maruzzi 1 Pisa 56124, Italy. E-mail: la.gizzi@ipcf.cnr.it

2. BASIC PRINCIPLES OF THE TECHNIQUE

In principle, the detection of a given element characterized by an absorption edge at a given wavelength, denoted by λ_{Edge}, requires two images of the sample to be taken using monochromatic radiation at two different photon wavelengths, one (λ_1) just below the edge wavelength, and another one (λ_2) just above the edge. Therefore the logarithmic subtraction of these two images gives directly a 2D map of the tracing element inside the sample.

More quantitatively, the 2D map of the intensity of the X-ray radiation transmitted by a sample irradiated at a normal incidence at a photon wavelength λ_j can be written as:

$$I^{(j)}(x, y) = I_0^{(j)}(x, y) \exp\left(-\sum_i \mu_i^{(j)} \int_s \rho_i(x, y, z)\, dz\right), \quad (1)$$

where z is the coordinate along the direction of the incident beam, x and y are the coordinates perpendicular to z, $I_0^{(j)}(x, y)$ is the incident beam intensity, with the index $j = 1,2$ identifying the two wavelengths, respectively, above and below the absorption edge, $\mu_i^{(j)}$ is the mass absorption coefficient of the i-th element in the sample at the j-th value of the wavelength, $\rho_i(x, y, z)$ is its density distribution and finally s is the thickness of the sample. Performing the logarithmic subtraction of the two distributions of intensity taken at the two photon wavelengths yields a map of the optical depth:

$$\Delta t(x, y) = \ln R = \sum_i \Delta \mu_i \int_s \rho_i(x, y, z)\, dz, \quad (2)$$

where $R = I^{(2)}(x, y) I_0^{(1)}(x, y) / I_0^{(2)}(x, y) I^{(1)}(x, y)$ and $\Delta \mu_i = \mu_i^{(1)} - \mu_i^{(2)}$ is the difference of the mass absorption coefficient of the element at the two wavelengths. For simplicity, we restrict our analysis to the case in which the two values of the photon wavelength are close enough to neglect the variation of the mass absorption coefficient of the other elements present in the sample, provided these elements do not exhibit an absorption edge in that wavelength range. This assumption sets a limit to the minimum detectable surface density of the tracing element in the sample. In this case, the surface mass density σ of the tracing element can be written as:

$$\sigma = \int_s \rho_i(z)\, dz = \frac{\ln R}{\Delta \mu}. \quad (3)$$

The uncertainty on the detectable surface mass density of the tracing element is obtained from Eq. (3) considering the uncertainties on $\Delta \mu$ and R, and can be written as:

$$\delta \sigma = \sqrt{\left(\frac{(\delta(\Delta \mu))}{\Delta \mu^2} \ln R\right)^2 + \left(\frac{\delta R}{R \Delta \mu}\right)^2}. \quad (4)$$

From an experimental viewpoint, the uncertainty on $\Delta \mu$ comes out to be negligible in comparison with the one concerning the measured intensities since tabulated values of μ are typically very accurate. Therefore, the uncertainty on the measurement of the surface mass density of a tracing element becomes:

$$\delta \sigma = \frac{\delta R}{R \Delta \mu}. \quad (5)$$

This corresponds also to the minimum detectable surface mass density, which will be denoted as σ_{min}, corresponding to the condition of a 100% relative error on the surface density ($\delta \sigma / \sigma = 1$).

3. THE CASE OF BROMINE

We will consider a sample containing a contrast agent consisting of Br whose L_2 edge ($\Delta \mu_{Br} = 1{,}506 \pm 10$ cm^2/g) is located at a wavelength of 7.7682 Å (1,596 eV). We will assume that the detection of X-rays is carried out using a cooled CCD X-ray detector. In these circumstances, the instrumental uncertainty on the transmitted X-ray beam intensity is given by the intensity resolution of the detector. In the case of a 14 bits detector, we have $\delta I = 6.2 \times 10^{-5}$, which leads to $\delta R / R \approx 1.24 \times 10^{-4}$. According to Eq. (5), these values give a minimum detectable surface mass density of $\sigma_{min} = 8.32 \times 10^{-8}$ g/cm^2. Assuming a sample thickness of 50 μm, a reasonable value of the X-ray attenuation length in the soft X-ray range for biological materials, we find that the minimum detectable average mass density is $\rho_{min} = 17$ μg/cm^3.

It should be pointed out here that in the case of the investigation of complex biological systems, the tracing element is usually found in well-localized (typically micrometer sized) regions with specific spatial properties (such as, interstitial regions, vessels, capillaries, etc). In these regions, the local concentration of the tracing element can be much higher than the average value. Consequently, provided sufficient spatial resolution is available in the imaging system, local concentrations of contrast agent can be detected even when average concentration values are well below the detectable value calculated above.

The use of Bromine as a test element for differential absorption studies requires X-ray radiation in the spectral region close to the Br L_2 edge. When using laser-plasma sources, X-ray emission in a given spectral range can be optimized by selecting the appropriate target material (Giulietti & Gizzi, 1998). In the case discussed here, K-shell emission from an Al plasma was selected which provides a number of spectral components in a range around the Br L_2 edge. Figure 1 shows the mass absorption coefficient of Br as a function of the wavelength. Also shown in the figure (dashed line) is an experimental spectrum of X-ray emission from an Al laser-plasma obtained using a slit-less flat crystal spectrometer (Labate *et al.*, 2001). The L_2 absorption edge of Br
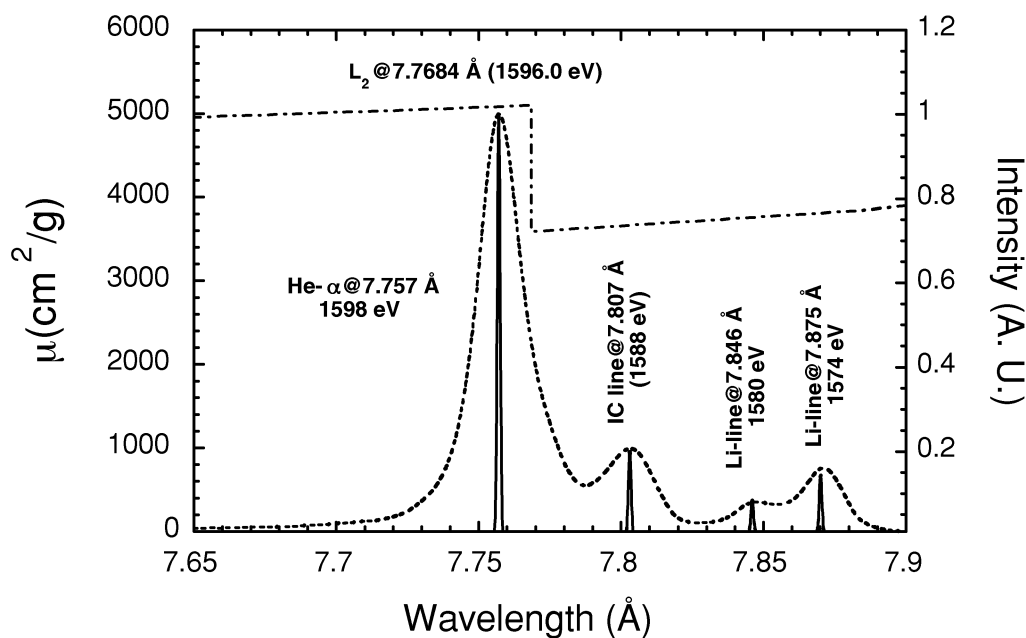
Fig. 1. Mass absorption coefficient of Br (dashed-dotted line) showing the L_2 absorption edge at 1596.0 eV. An experimental X-ray spectrum of K-shell Al emission around the absorption edge is also shown (dashed line). The solid line shows the same plot calculated assuming a line-width of 1 mÅ (see text).

is located just between some of the most intense K-shell Al lines. The bright line below the edge is the $1s^2$ ^{1}S–$1s2p$ ^{1}P transition line from the He-like Al (the so-called He-α resonance line) located at 7.757 Å (1,598 eV). The brightest lines above the edge are the $1s^2$ ^{1}S–$1s2p$ ^{3}P (the so-called intercombination (IC) line) at 7.807 Å (1,588 eV), and the Li-like $1s^2 2p$–$1s2p^2$ at 7.875 Å (1,574 eV). The IC line, while being closer to the edge and therefore being a better candidate than the Li-like line at $\lambda_2 = 7.875$ Å, is more sensitive to changes in the physical plasma conditions and therefore its intensity is subject to larger shot-to-shot fluctuations. For this reason, the Li-like $1s^2 2p$–$1s2p^2$ at $\lambda_2 = 7.875$ Å ($E_2 = 1574$ eV) is a more reliable emission line.

The width of these two X-ray lines as shown in Figure 1 is mainly due to instrumental and geometrical factors originating from the finite size of the X-ray emitting region. From the point of view of our imaging application, one should consider the actual transition line-width which is essentially determined by the Doppler effect arising from the thermal motion of the emitting ions. For an Al plasma at a temperature of the order of 100 eV, the relative width of an emitting line ($\Delta\lambda/\lambda$) is of the order of 10^{-4}. Therefore, one should expect an effective line-width as shown by the solid line in Figure 1. We can therefore conclude that the He-α and Li lines are sufficiently well-separated and monochromatic to be considered good candidates for differential absorption measurements across the L_2 edge of Br.

4. EXPERIMENTAL SET-UP

A schematic view of the experimental set up is shown in Figure 2. X-ray radiation emitted from the source (K-shell

emission from an Al target plasma) is collected using a spherically bent mica crystal set up in such a way that the X-ray source is located on the Rowland circle (that is, the circle of diameter equal to the radius of curvature of the crystal). In such a configuration, the crystal acts as a monochromator and consequently, a highly monochromatic beam is Bragg-reflected on the CCD detector. The crystal is placed on a remotely controlled mount that can perform rotation on
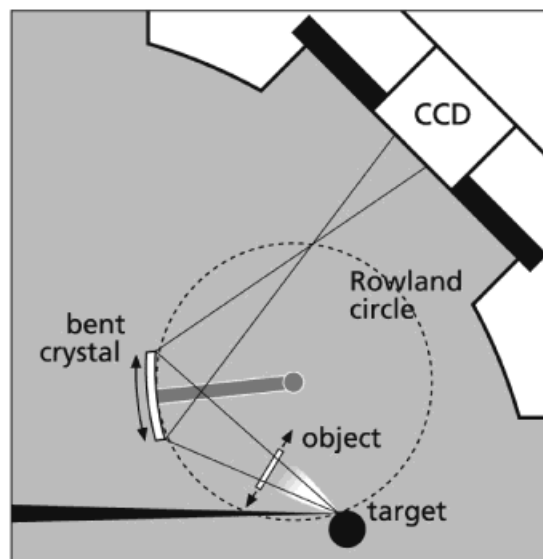
Fig. 2. Experimental set-up for monochromatic imaging of thin samples using a laser-plasma X-ray source. The geometry of the imaging system is based upon a spherically bent crystal set up according to so-called Shadow Monochromatic Backlighting configuration (Pikuz *et al.*, 2001).

the Rowland circle. This enables the X-ray wavelength to be tuned according to the Shadow Monochromatic Backlighting set up presented in detail in (Pikuz *et al.*, 2001; Sanchez del Rio *et al.*, 2001). A comprehensive description and modeling of the crystal imaging system is given by Labate *et al.* (2004). Here we present the main experimental results concerning the implementation of this system for differential absorption micro-imaging.

Figure 3 shows the beam pattern produced by the crystal (behaving as a monochromator) tuned on the $1s^2$-$1s2p$ He-α line mentioned earlier. The IC line and the Li-like lines are also just visible on the left-side of the main component. A small rotation of the crystal enables the beam photon wavelength to be tuned on a different value, while still keeping the sample on the X-ray beams.

When a sample is placed between the source and the crystal, as shown in Figure 2, a micrometer-resolution radiography of the sample at the selected photon wavelength is generated. The image of Figure 4 shows a micro-imaging resolution test carried out on the system using an object consisting of a Fresnel zone-plate ($\lambda f = 0.114$ mm^2, radius of the first opaque zone equal to 340 μm) whose total diameter was 7.5 mm. According to this test we can find that, in our experimental conditions, the spatial resolution in the horizontal direction is about 15 μm while in the vertical direction its value is about 40 μm. A comprehensive discussion on the spatial resolution properties of this imaging system can be found elsewhere (Labate *et al.*, 2004).

5. RESULTS AND DISCUSSION

A sample containing Bromine as a test element was prepared (see Figure 5) using a water solution of LiBr of a known concentration of 0.265 g/ml. An amount of 0.2 μl of the solution was deposited on the 30 μm thick paper substrate and the water was then removed in vacuum. The sample was mounted on a washer and placed between the source and the crystal as indicated in Figure 2. Taking into account the absorption properties of Br and considering the parameters of the sample, a simple calculation gives an
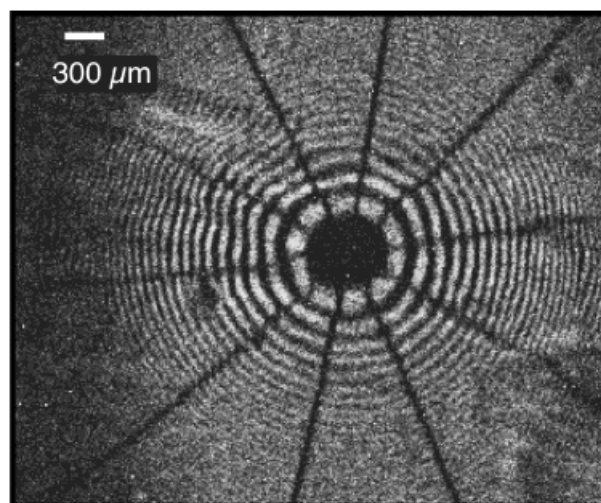

Fig. 4. Monochromatic micro-imaging resolution test of the Shadow Monochromatic Backlighting set-up tuned at 7.757 Å ($1s^2$–$1s2p$ He-α) using a Fresnel zone-plate ($\lambda f = 0.114$ mm^2, radius of the first opaque zone equal to 340 μm, total diameter is 7.5 mm).

average surface mass density of 6×10^{-4} ($\pm 7 \times 10^{-5}$) g/cm^2 and a corresponding optical depth difference of $\Delta t = 0.9 \pm 0.1$.

The raw experimental results are shown in Figures 6a and b. The upper images of (a) and (b) show, respectively, the incident X-ray beam, that is, the beam without the sample, at the two wavelengths below ($\lambda_1 = 7.757$ Å) and above ($\lambda_2 = 7.785$ Å) the L_2 absorption edge of Br. These images were obtained integrating the CCD image over 10 X-ray pulses (10 shots of the driving laser) at 10 Hz, corresponding to a total time of exposure of 1 s. The lower images of (a) and (b) show the X-ray beam transmitted through our sample for the same two wavelengths obtained integrating over 300 X-ray pulses (which corresponds to 30 s of exposure).

The transmitted image of the sample consists of a circular region (inside the washer) with an inner, irregularly shaped darker (optically thicker) region due to the LiBr deposit. The parallel darker lines visible on the images are a consequence
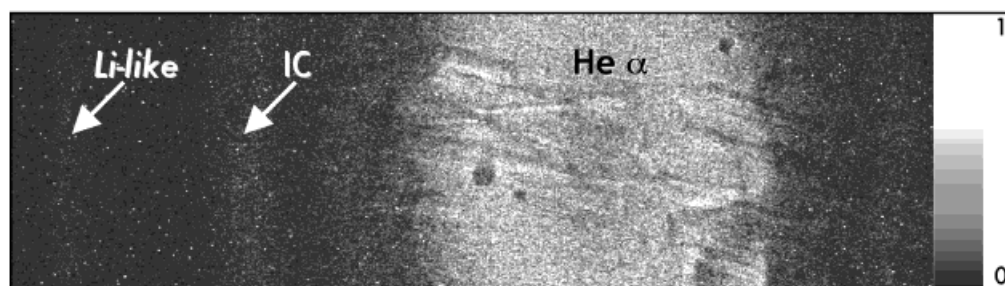
Fig. 3. CCD image of the monochromatic X-ray beam as obtained with the experimental configuration shown in Figure 2. The crystal was tuned on the $1s^2$–$1s2p$ (He-α transition line from the He-like Al). The Li-like transition line and the intercombination line are also visible.
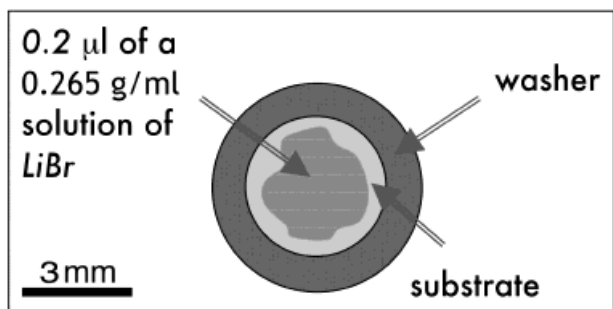
Fig. 5. Schematic view of the sample consisting of a solution of LiBr deposited on the 30 μm thick paper substrate mounted on a washer.

of the fiber-like structure of the paper substrate that results in modulations of the paper thickness, and consequently, modulations on the transmitted intensity. Finally, the shadow due to the washer used to hold the sample is also visible.

A quantitative analysis of these results has been carried out using Eq. (1) and averaging the result on the area of the sample containing the LiBr deposit. The measurements give an average optical depth difference $\Delta t = 1.1 \pm 0.8$ that corresponds to a surface mass density $\sigma = 7.3 \times 10^{-4}$ ($\pm 5 \times 10^{-4}$) g/cm^2. Such a value of optical depth difference is in agreement with the value of $\Delta t = 0.9 \pm 0.1$ expected from the presence of Br. The large uncertainty found in our measurements, compared with the uncertainty given by Eq. (3) is partly due to the single-photon noise arising from diffuse X-ray scattering, especially for the measurement at the photon energy above the edge, where too high absorption from Br occurs. In view of these considerations, higher signal-to-noise ratios should be obtained for samples with a much lower surface density, as in the case of real tracing concentrations.

This result should also be considered in view of the fact that the other known elements present in the sample with
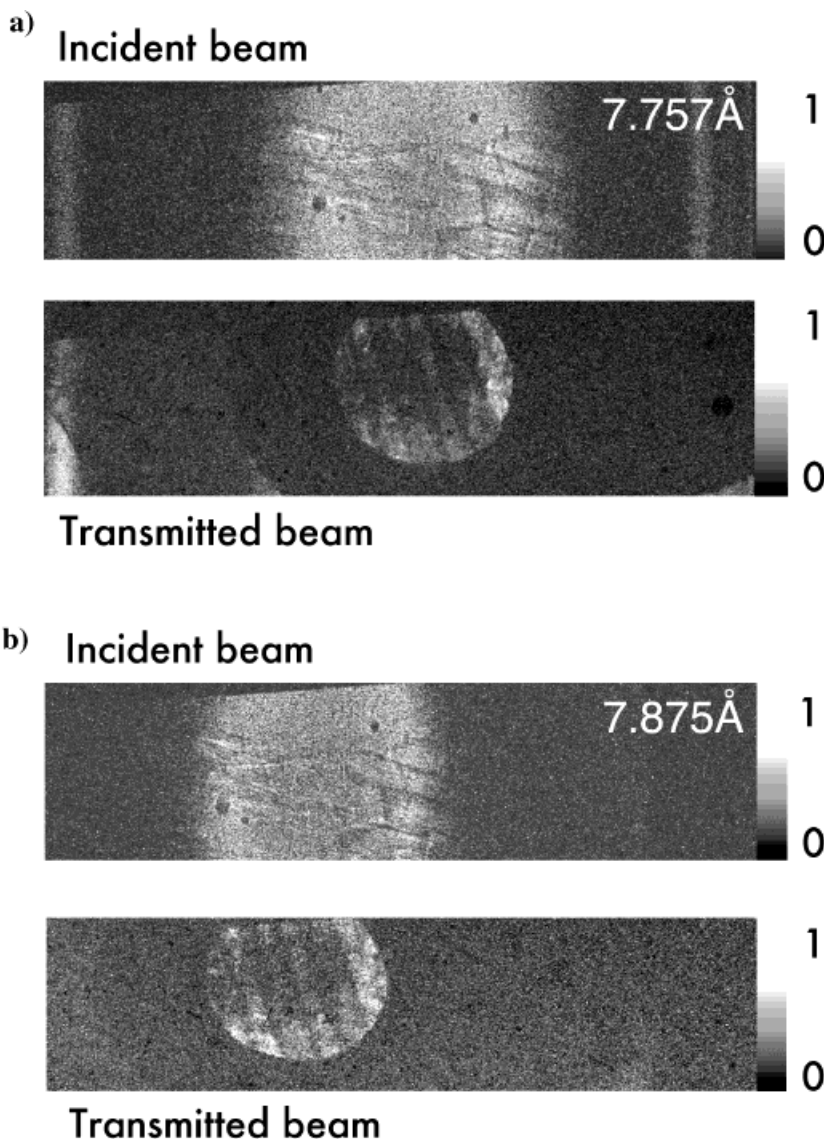

Fig. 6. a–b. Experimental data of the differential absorption experiment on the LiBr sample used in our experiments. Images (a) were taken at the wavelength (7.75 Å) below the L$_2$ absorption edge of Br: the highest one show the X-ray beam without the sample and the other one for the transmitted X-ray beam through the sample. The lowest ones (b) are taken above (7.87 Å) the L$_2$ edge.

substantial abundances (e.g., Li, C, H, O) exhibit a smooth change, but no absorption edges, of the mass absorption coefficient between the two wavelengths considered here. Consequently, the change of optical depth expected for the presence of elements other than Br is negligible. Indeed, a simple estimate shows that, in the presence of a smooth variation of the mass absorption coefficient, a change of 10 eV in the photon beam energy corresponds to a typical change of the mass absorption coefficient of approximately less than 100 cm^2/g and, according to Eq. (2), a corresponding difference in the optical depth smaller than 0.1, that is, approximately 10 % of the value expected for Bromine.

6. SUMMARY AND CONCLUSIONS

In this paper, we have shown that our technique based on differential imaging using a laser-plasma soft X-ray source combined with crystal optics enabled us to detect the presence of Br in a thin sample. In fact, we were able to detect a significant change in the optical depth of the sample by changing the imaging X-ray wavelength by less than 100 mÅ. Moreover, our measurement enabled us to measure the surface density of Br in our test sample.

Important issues need to be addressed in order to make this method a general purpose technique for the detection of trace-level elements in thin samples. The main aspect concerns the possibility of extending the range of applicability to other absorption edge wavelengths, that is, other elements. To this purpose, suitable emission photon energies close to the absorption edge under investigation can be identified. On the other hand, the possibility of using a laser-driven plasma source may result in an easy access to the technique on the basis of a small scale dedicated laboratory. This may result in the possibility of improving the image quality and spatial resolution of widely used techniques like self-emission radiography. On the other hand, the possibility of using non-radioactive tracing elements opens new possibilities for radioactivity-free laboratory diagnostics in medicine and biology.

ACKNOWLEDGMENTS

REFERENCES

ANDERSSON, E., HÖLZER, G., FÖRSTER, E., GRÄTZ, M., KIERNAN, L., SJÖGREN, A. & SVANBERG, S. (2001). Coronary angiography using laserplasma sources: X-ray source efficiency and optimization of a bent crystal monochromator. *J. Appl. Phys.* **90**, 3048.

BARBARICS, E., KRONAUGE, J.F., COSTELLO, C.E., JANOKI, G.A., HOLMAN, B.L., DAVISON, A. & JONES, A.G. (1994). In-Vivo Metabolism Of The Technetium Isonitrile Complex [Tc(2-Ethoxy-2-Methyl-1-Isocyanopropane)(6)](+). *Nuclear Medicine And Biology*, **21**, 583.

DILL, T., DIX, W.-R., HAMM, C.W., JUNGZ, M., KUPPER, W., LOHMANN, M., REIME, B. & VENTURA, R. (1998). Intravenous coronary angiography with synchrotron radiation. *Eur. J. Phys.* **19**, 499.

GIULIETTI, D. & GIZZI, L.A. (1998). X-ray emission from laser-produced plasmas. *La Rivista del Nuovo Cimento* **21**, 1.

LABATE, L., GALIMBERTI, M., GIULIETTI, A., GIULIETTI, D., GIZZI, L.A., NUMICO, R. & SALVETTI, A., LINE SPECTROSCOPY WITH SPATIAL RESOLUTION OF LASER-PLASMA X-RAY EMISSION. *Laser and Part. Beams* **19**, 117.

LABATE, L. *et al.* (2004). Ray-tracing simulations of an X-ray optics based upon a bent crystal for imaging using laser-plasma X-ray sources. *Laser Part. Beams* **XX**, XX.

MARZI, S., GIULIETTI, A., GIULIETTI, D., GIZZI, L.A. & SALVETTI, A. (2000). A High Brightness Laser-Plasma X-ray source at IFAM: Characterisation and applications. *Laser and Part. Beams* **18**, 109.

PIKUZ, T.A. *et al.* (2001). *Laser Part. Beams* **19**, 285.

SANCHEZ DEL RIO, M. *et al.* (2001). *Rev. Sci. Instrum.* **72**, 3291.

SUORTTI, P. & THOMLINSON, W. (2003). Medical applications of synchrotron radiation. *Phys. Med. Biol.* **48**, R1.

TILLMAN, C., MERCER, I. & SVANBERG, S. (1996). Elemental biological imaging by differential absorption with laser-produced x-ray source. *J. Opt. Soc. Am. B* **13**, 209.